EFFECTS OF FLARES ON SOLAR OSCILLATION CHARACTERISTICS

Ashok Ambastha[1], Sarbani Basu[2], and H. M. Antia[3]

[1]Udaipur Solar Observatory, Physical Research Laboratory, P. O. Box 198, Udaipur 313001, India
[1]email: ambastha@prl.ernet.in
[2]Astronomy Department, Yale University, P. O. Box 208101, New Haven CT 06520-8101, U. S. A.
[2]email: basu@astro.yale.edu
[3]Tata Institute of Fundamental Research, Homi Bhabha Road, Mumbai 400005, India
[3]email: antia@tifr.res.in

ABSTRACT

We use ring diagram analysis to study the effects of solar flares on p-mode oscillation characteristics. We study the changes in the amplitude, frequency and width of acoustic modes using data before, during and after a few of the major flares during the current solar cycle. Mode power is found to be enhanced during and after some flares, though the enhancement is not seen in all flares.

Key words: Sun: oscillations; Sun: activity.

1. INTRODUCTION

Solar flares are amongst the most energetic phenomena observed on the solar surface. There have been observations (Kosovichev & Zharkova 1998, 1999) suggesting that some large flares excite waves on the solar surface. Most of the flare energy is emitted in the chromosphere and corona, however, some white light flares suggest that there may still be substantial energy released in the photosphere which can affect the solar oscillations. In order to study the effect of flares on solar oscillation modes we use the ring diagram technique (Hill 1988; Patrón et al. 1997; Basu et al. 1999) applied to 3D spectra from the MDI instrument. We use spectra obtained before, during and after the flares to study if there is any variation in mode characteristics such as frequency, width, power and asymmetry.

2. DATA AND TECHNIQUE

To study the effect of flares, we have chosen 10 active regions that had flares when they were close to the central meridian. Major flares from these regions around the time covered by our study are given in

Table 1. Characteristics of solar Active Regions (AR) and Flares

NOAA No.	L0	Area ($10^{-6}A_\odot$)	Flare Class SXR/H_α	Location	Date	Start (UT)	End (UT)
8179	032	0800	M1.8/1B	S21W03	15MAR98	19:11	19:27
8185	231	0530	M1.8/2B	S26E19	26MAR98	12:46	13:40
	232	0430	M2.4/3N	S24W03	27MAR98	21:49	23:17
8485	276	0610	M6.2/2N	N23W39	16MAR99	21:34	21:46
8525	300	0260	M4.4/2N*	N15E32	03MAY99	05:36	06:32
8539	227	0010	M2.5/2N	N16E19	10MAY99	05:22	05:37
9026	075	0260	M7.6/3B	N16E60	02JUN00	18:48	19:50
	076	0720	M2.1/1F	N19E54	03JUN00	08:27	08:58
	076	0720	M6.1/2B	N20E49	03JUN00	19:13	19:32
	074	0820	X1.1	N21E23	06JUN00	13:30	13:46
	074	0820	M7.1		06JUN00	13:56	14:11
	074	0820	X2.3	N19E14	06JUN00	14:58	15:40
	074	0800	X1.2/3B*	N23E03	07JUN00	15:34	16:06
9046	252	0310	M2.6/2B	N19W30	23JUN00	04:00	04:12
9393	150	0820	M2.5/2N	N17E51	25MAR01	04:12	04:31
	150	0820	M2.6/1N	N21E59	25MAR01	10:33	11:20
	152	1040	M2.7/1N	N20E51	26MAR01	02:28	02:46
	151	1100	M2.2/1N	N21E33	27MAR01	16:25	16:32
	153	1590	M4.3/SF	N18E02	28MAR01	11:21	13:06
	153	1590	M1.6/1N	N17W01	28MAR01	22:18	22:55
	151	2240	X1.7/1B	N20W19	29MAR01	09:57	10:32
9415	358	0710	X5.6/SF	S21E31	06APR01	19:10	19:31
	001	0790	M7.9/2B	S21W04	09APR01	15:20	16:00
	359	0760	X2.3/3B*	S23W09	10APR01	05:06	05:42
	358	0490	M2.3/1F	S22W27	11APR01	12:56	13:49
	357	0550	M1.3/1N	S22W38	12APR01	02:56	03:29
	357	0550	X2.0/SF	S19W43	12APR01	09:39	10:49
9433	154	0880	M4.0/2N	N14E23	23APR01	20:15	20:43
	156	1070	M7.8/2B*	N17W31	26APR01	11:26	13:19

Table 1. We have calculated flare indices for the selected active regions using the quantity $Q = i \times \tau$ to quantify the daily flare activity summed over the duration of tracked data sets using the method described by Kleczek (1952), and Atac & Ozguc (1998). This relationship gives an approximate estimate of the total energy emitted by the flares in the active region. In this relation, i is the intensity scale of the importance, and τ is the duration of the flare in minutes. This flare index (FI), along with other properties of regions studied is given in Table 2. The Table also list the Magnetic Activity Index (MAI)

Proc. of SOHO 12/GONG+ 2002 'Local and Global Helioseismology: The Present and Future', Big Bear Lake, California (U.S.A.), 27 October – 1 November 2002 (ESA SP-517, February 2003)

(see Rajaguru et al. 2001 for definition) which is a measure of the average surface magnetic field in the region.

NOAA 9393 was the largest active region observed in the last 20 years. It produced 23 M and 5 X class flares (including the largest X20 flare of Solar Cycle 23) during its disk transit of March 24–April 5, 2001. It possessed a very large MAI value (184.8 G). Out of the two large proton flares, the X1.7/1B event on March 29, 2001/10:15 UT occurred when the AR was close to the disk-centre at N20W19, making it favourable for solar oscillation characteristics studies. NOAA9026 produced two proton flares, an X2.3/3B event on June 06, 2000/15:25 UT, and a M5/3B event on June 10, 2000/17:02 UT, respectively. Both these events were associated with halo CMEs. The event of June 6, 2000 was well covered by MDI data sets, when an additional X-class, and an M-class flare also occurred. These events correspond to a large flare index, FI = 1783, which is the largest in our study.

In order to study the effect of flares on solar oscillation modes, we use the ring diagram analysis technique on data sets from MDI. Each of the data sets covers a region of about 16° × 16° on the Sun and a time interval of 1664 minutes. We have chosen the data from available sets when the active region was close to central meridian. The data sets used are listed in Table 2. This table gives the heliographic coordinates of the central point as well as the central meridian longitude at midpoint in time. For convenience each region is identified by the serial number listed in the first column. We take the 3D spectra of oscillation power for each of the regions. Mode characteristics are known to be affected by magnetic fields in active regions (Rajaguru et al. 2001) and hence we need to account for differences in MAI values of different regions. In particular, the power in modes is known to reduce as the MAI increases.

To fit the 3d spectra we use a model with asymmetric peak profiles as used by Basu & Antia (1999)

$$P(k_x,k_y,\nu) = \frac{e^{B_1}}{k^3} + \frac{e^{B_2}}{k^4} + \frac{\exp(A_0 + (k-k_0)A_1 + A_2(\frac{k_x}{k})^2 + A_3\frac{k_xk_y}{k^2})S_x}{x^2+1} \quad (1)$$

where

$$x = \frac{\nu - ck^p - U_xk_x - U_yk_y}{w_0 + w_1(k-k_0)}, \quad (2)$$

$$S_x = S^2 + (1+Sx)^2, \quad (3)$$

and the 13 parameters $A_0, A_1, A_2, A_3, c, p, U_x, U_y, w_0, w_1, S, B_1$ and B_2 are determined by fitting the spectra using a maximum likelihood approach (Anderson et al. 1990). The parameter S measures the asymmetry in the peak profile. The form of asymmetry is the same as that used by Nigam & Kosovichev (1998). The mode characteristics we are interested in are the frequency (ck^p), peak power ($\exp(A_0)$), half-width (w_0) and asymmetry parameter S.

Table 2. Regions studied using ring diagram analysis

No.	Lat.	Lon.	CM Lon.	Start time	End time	MAI (G)	FI
NOAA 8179 Carrington rot 1933 (March 1998)							
R01	22.5S	30	060	13/00:38	14/04:21	39.0	4.5
R02	22.5S	30	045	14/03:56	15/07:39	70.8	66.0
R03	22.5S	30	030	15/07:13	16/10:56	91.2	306.0
R04	22.5S	30	015	16/10:31	17/14:14	100.9	332.0
NOAA 8185 Carrington rot 1934 (March 1998)							
R10	22.5S	225	255	25/12:52	26/16:35	49.3	172.0
R11	22.5S	225	240	26/16:10	27/19:53	47.6	10.0
R12	22.5S	225	225	27/19:27	28/23:10	48.5	302.5
R13	22.5S	225	210	28/22:44	30/02:27	49.9	9.5
R14	22.5S	225	195	30/02:02	31/05:45	48.8	0.0
NOAA 8485 Carrington rot 1947 (March 1999)							
R20	22.5N	270	315	10/13:14	11/14:58	41.7	29.0
R21	22.5N	270	285	13/00:59	13/23:34	49.0	40.0
R22	22.5N	270	270	13/23:09	15/02:52	59.9	59.0
R23	22.5N	270	255	15/02:28	16/06:11	60.5	43.5
R24	22.5N	270	240	16/05:46	17/09:29	61.1	375.0
R25	22.5N	270	225	17/09:04	18/12:47	58.2	105.5
NOAA 8525 Carrington rot 1949 (May 1999)							
R30	15.0N	300	345	01/20:17	03/00:00	54.9	50.0
R31	15.0N	300	330	02/23:33	04/03:16	54.6	253.5
R32	15.0N	300	315	04/02:48	05/06:31	60.2	13.5
R33	15.0N	300	300	05/06:03	06/09:46	63.7	16.0
R34	15.0N	300	285	06/09:18	07/13:01	64.8	18.5
R35	15.0N	300	270	07/12:33	08/16:16	62.6	117.0
R36	15.0N	300	255	08/15:47	09/19:30	53.9	3.0
NOAA 8539 Carrington rot 1949 (May 1999)							
R40	15.0N	225	255	08/15:47	09/19:30	28.4	0.0
R41	15.0N	225	240	09/19:02	10/22:45	28.7	102.0
R42	15.0N	225	225	10/22:17	12/02:00	26.4	0.0
R43	15.0N	225	195	13/04:46	14/08:29	20.8	0.0
NOAA 9026 Carrington rot 1963 (June 2000)							
R50	22.5N	75	105	04/19:58	05/23:41	113.1	93.5
R51	22.5N	75	090	05/23:10	07/02:53	113.2	1793.0
R52	22.5N	75	075	07/02:23	08/06:06	104.4	895.0
R53	22.5N	75	060	08/05:35	09/09:18	92.3	132.0
R54	22.5N	75	045	09/08:47	10/12:30	72.1	52.0
NOAA 9046 Carrington rot 1964 (June 2000)							
R60	22.5N	255	285	18/10:24	19/14:07	103.2	3.5
R61	22.5N	255	270	19/13:35	20/17:18	99.4	28.5
R62	22.5N	255	255	20/16:47	21/20:30	98.4	28.5
R63	22.5N	255	240	21/19:59	22/23:42	89.8	75.5
R64	22.5N	255	225	22/23:11	24/02:54	75.0	170.5
R65	22.5N	255	210	24/02:22	25/06:05	54.9	16.5
NOAA 9393 Carrington rot 1974 (March–April 2001)							
R74	15.0N	150	195	25/02:12	26/05:55	104.0	126.5
R75	15.0N	150	165	27/08:48	28/12:31	168.4	302.0
R76	15.0N	150	150	28/12:07	29/15:50	184.8	499.5
R77	15.0N	150	135	29/15:25	30/19:08	184.5	296.5
R78	15.0N	150	120	30/18:43	31/22:26	168.5	103.5
R79	15.0N	150	105	31/22:01	02/01:44	154.4	144.5
NOAA 9415 Carrington rot 1975 (April 2001)							
R80	22.5S	000	015	07/17:57	08/21:31	111.1	3.5
R81	22.5S	360	360	08/21:05	10/00:48	112.1	373.5
R82	22.5S	360	345	10/00:23	11/04:06	108.7	881.0
R83	22.5S	360	330	11/03:40	12/07:23	97.1	238.0
R84	22.5S	360	315	12/06:57	13/10:40	83.8	229.0
NOAA 9433 Carrington rot 1975 (April 2001)							
R90	15.0N	150	180	22/12:27	23/16:10	101.2	233.0
R91	15.0N	150	165	23/15:43	24/19:26	107.3	474.0
R92	15.0N	150	150	24/18:59	25/22:42	110.6	329.0
R93	15.0N	150	135	25/22:15	27/01:58	104.0	452.0
R94	15.0N	150	120	27/01:31	28/05:14	94.0	165.0

3. RESULTS

Fig. 1 summarises the results for each of the 10 ARs that we have studied. The lowest panel in each figure shows the evolution of MAI and the Flare index as calculated by us. The horizontal axis is the serial number of the regions, which are separated generally at intervals of about 1 day. The upper panels show the evolution of amplitude and width of modes. For this purpose we have taken an average over all modes

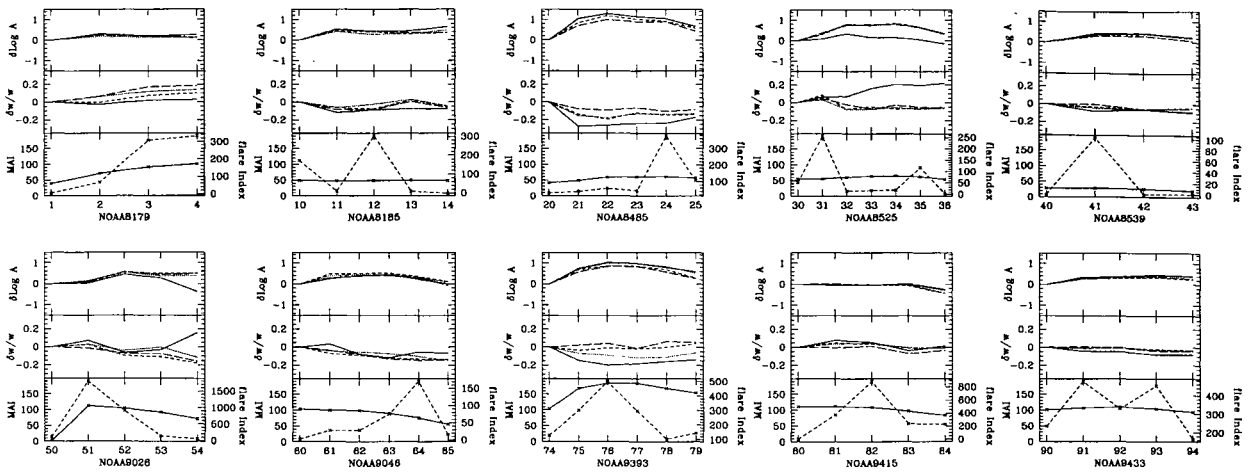

Figure 1. The evolution of MAI and flare index for each of the regions is compared with evolution of mode characteristics like, amplitude and width of modes. In the lowest panels solid line shows MAI values, while the dashed line shows the flare index. In the upper two panels the solid, dotted, short-dashed and long-dashed lines respectively, show the results for $n = 0, 1, 2, 3$ modes. The amplitude and width are averaged over all modes in frequency range of 2.5–3 mHz for f-modes ($n = 0$) and over 3–3.5 mHz for p-modes ($n > 0$).

in frequency interval 2.5–3.0 mHz for f-modes ($n = 0$) and in interval 3.0–3.5 mHz for p-modes ($n > 0$). All differences shown in the figures are with respect to the first region.

For the active region NOAA9393 the largest flare occurred in region R76, when the region was close to the central meridian. The magnetic field did not evolve significantly around that time. The mode-amplitudes are found to be maximum for R76 which also has the highest MAI value. The mode-amplitudes increase from region R74 to R75, even though the MAI also increased. This was unexpected, since as mentioned before, non-flare active regions showed a *decrease* in mode-amplitudes with increase in MAI (Rajaguru et al. 2001). This increase is likely to be due to flares that occurred during R75. After that the mode-amplitudes remained essentially constant until R78 even though more flares had taken place. During R79 the mode-amplitudes are substantially reduced even though the MAI value had reduced. Thus the effect of MAI appears to be compensated by that of the flares. The width of the modes has also reduced during the flare.

Fig. 2 shows the difference in mode characteristics in the region covered by NOAA9393 at different times. The frequencies are not significantly affected during this period, however, the small difference that is seen is of opposite sign before and after the flare. The frequency differences are positive for post flare spectra which may be expected from the fact that magnetic field is highest in region R76. But in the preflare spectra although the magnetic field is smaller the frequency differences are negative, which is contrary to expectation. This could be due to complex changes taking place before the flare. Most of the change in frequency occurs for high-frequency modes which suggests that changes are confined to outermost layers close to the photosphere.

In order to check if similar effects are seen in other flares we look at the data from NOAA9026. This region has the largest flare index amongst all region studied and the magnetic field had not changed significantly during the period under consideration. The power in oscillations appears to have increased after region R51 which had the largest flare. The region R52 also had a substantial flare index and shows maximum mode-amplitude, which could be due to flares. The mode-amplitudes for R52 is found to be larger than that for R51 which had a larger flare activity. It is possible that the effect of the large flare in R51 persisted for some time. In this case too, the width of the modes decreased after the flare. The frequency difference is also found to be similar to that for NOAA9393.

The active region NOAA8539 had a minor flare during R41 and very little flare activity during other times. The magnetic field in this region was also rather low. Despite this it shows enhanced power during R41 and R42, which could be due to the flare. The width of modes also reduced, like in other cases.

The active region NOAA8485 had a flare during R24 and also showed a slow increase in the magnetic field during this period. The mode-amplitudes increased substantially between R21 and R20, but started declining after R22, despite the flare. It is not clear what the effect of the flare was in this case.

The active region NOAA9415 had a major flare during R82, but the mode-amplitudes were essentially constant over the interval R80–R83. The magnetic field for this AR decreased substantially after the flare. It is possible that amplitude increase due to reduction in magnetic field was compensated by

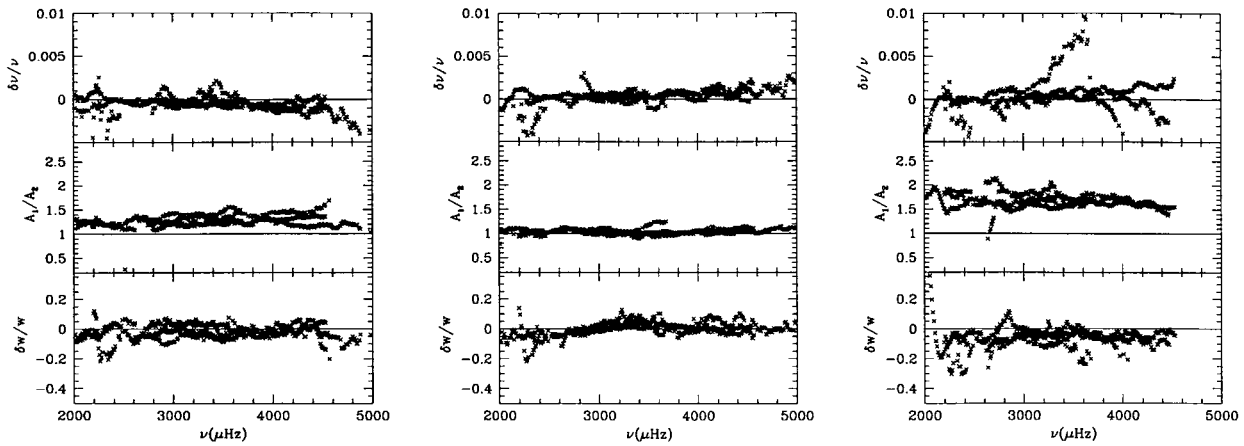

Figure 2. The relative difference in mode frequencies, and widths as well as ratio of peak power for the active region NOAA9393 when it is away from the central meridian. The left to right panels respectively, show the difference between regions $R76 - R75$, $R76 - R77$ and $R76 - R79$.

amplitude-enhancement due to the flares.

The active region NOAA8179 had a flare during R3 and R4 and also had a significant increase in magnetic field during this time. In this case there was very little variation in the power in the modes. It is possible that the power enhancement due to flares was compensated by the reduction in power expected from the increase in the MAI.

4. CONCLUSIONS

During some flares the power in acoustic modes appears to increase beyond the normal value expected from the influence of magnetic field. The frequencies of high degree modes appear to be reduced before some flares. This could be due to either change in structure of this region or complex magnetic field variation leading to flares. These changes should be confined to outermost layers around the photosphere. These signatures are not seen in all flares and there is considerable variation between different flares. The extent by which the power appears to be enhanced by flares does not have any obvious correlation with the flare index.

The observed variations in the effect of flares may perhaps be attributed to the relative amounts of deposited flare energy at the lower and deeper layers, and particularly in the photosphere. The large X-class of flare alone is not an adequate indicator of this deposition, as this parameter is related mainly to the emission from the higher, coronal level. On the other hand, a lower X-class, but higher H_α class of the flare may be more important when it comes to effects on oscillation modes. Similarly, it may be expected that the rather rare, white-light flares should excite the p-modes significantly. The flare index alone may not be a good indicator of the magnitude of flare, in affecting the photosphere. In fact, a large FI may result due to several long duration, but small magnitude flares integrated over the time-interval of MDI data. On the other hand, it is possible that a very impulsive flare, which would be more important, was of rather short duration, thereby giving a smaller FI. Much more work is needed to understand the flare to flare variations.

ACKNOWLEDGEMENTS

This work was supported in part by NASA Grant NAG5-10912 to SB. This work utilises data from the Solar Oscillations Investigation/ Michelson Doppler Imager (SOI/MDI) on the Solar and Heliospheric Observatory (SOHO). SOHO is a project of international cooperation between ESA and NASA. MDI is supported by NASA grants NAG5-8878 and NAG5-10483 to Stanford University.

REFERENCES

Anderson E. R., Duvall T. L., Jr., Jefferies S. M. 1990, ApJ 364, 699

Atac T., & Ozguc A. 1998, Solar Phys. 180, 397.

Basu S., Antia H. M. 1999, ApJ 525, 517

Basu S., Antia H. M., Tripathy S. C. 1999, ApJ 512, 458

Hill F. 1988, ApJ 333, 996

Kleczek J. 1952, Publ. Inst. Centr. Astron. Prague, No. 22

Kosovichev A. G., Zharkova V. V. 1998, Nature 393, 317

Kosovichev A. G., Zharkova V. V. 1999, Solar Phys. 190, 459

Nigam R., Kosovichev A. G. 1998, ApJ 505, L51

Patrón J., González Hernández I., Chou D.-Y., et al. 1997, ApJ 485, 869

Rajaguru S. P., Basu S., Antia H. M. 2001, ApJ 563, 401